Dynamic coding of choice targets in the perirhinal cortex

Tomoya Ohnuki *, Yuma Osako, Hiroyuki Manabe, Yoshio Sakurai, Junya Hirokawa *

Laboratory of Neural Information, Graduate School of Brain Science, Doshisha University, 1-3 Tatara Miyakodani, Kyotanabe, Kyoto, 610-0394, Japan.

*Correspondence and requests for materials should be addressed to T.O. (kdp1003@mail4.doshisha.ac.jp) and J.H. (jhirokaw@mail.doshisha.ac.jp).

Abstract

Cortical neurons flexibly respond to multiple task-events characterized by distinct computational aspects. There are two possible explanatory scales, dynamic population code realizing computational flexibility and single-neuron code associating relevant information across task events. Since these interpretations were independently developed, it is unclear how neurons contribute to population dynamics with their individual ability to integrate relevant information. Here we show systematic changes in single-neuron representations of choice targets shape population dynamics. We analyzed neural activities in the perirhinal cortex while rats performed a two-alternative target-choice task. A time-resolved pattern analysis indicated dynamic population code of choice targets with two time-stable states during the cue and reward periods. The population patterns during these periods were substantially reversed and therefore allowed us to decode task-periods as well as choice targets. Our results clarify the contribution of single-neuron representations to population dynamics, suggesting its potential advantages such as reconciling different computational demands.

Introduction

Individual neurons across cortical areas show temporally flexible responses to multiple task-events characterized by different computational aspects, such as cue, action and reward (e.g., **Sakurai et al, 2017; Sakurai, 1990a,b**). Recent studies indicate that such complex single-neuron responses are only interpretable in terms of their contribution to population dynamics which flexibly perform different computations, particularly in association and motor cortices (**Elsayed et al., 2016; Lara et al., 2018; Mante et al., 2013; Raposo et al., 2014**). On the other hand, in some cortical areas, it has been shown that individual neurons respond to multiple task-events while reflecting their associations (Perirhinal cortex: **Eradath et al., 2015**, Motor cortex: **Guo et al., 2017**, Insular cortex: **Gardner and Fontanini, 2014**, Anterior cingulate cortex: **Kennerley and Wallis, 2009**, and Orbitofrontal cortex: **Furuyashiki et al., 2008; Hirokawa et al., 2017; Hosokawa et al., 2005**), suggesting that some cortical neurons afford to integrate relevant information across different task-events. Therefore, it is still an open question how such neurons contribute to population dynamics which would be suitable for differentiating task events.

In the present study, we explored neural activities in the perirhinal cortex (PRC) which has been implicated in association memory of objects (**Ahn and Lee, 2017, 2015; Naya et al., 2003a, 2003b, 1996; Sakai and Miyashita, 1991**). This region receives sensory inputs from almost all modalities, behavioral context information from the prefrontal cortex and reward-related signals from the amygdala (**Burwell, 2001; Burwell and Amaral, 1998; Furtak et al., 2007; Tomás Pereira et al., 2016**), creating integrated object representations (**Ohyama et al., 2012; Qu et al., 2016; Taylor et al., 2006**). Some studies show that some PRC neurons respond to the same visual cue across time contexts but in different degrees of strength (**Naya et al., 2017; Naya and Suzuki, 2011**). Therefore, it is possible that the PRC is able to represent the same target even across explicitly different task-events such as cue, action and reward, while differentiating those task-events.

To determine this possibility and elucidate underlying mechanisms, we analyzed single-unit activities recorded from the PRC while rats performed a two-alternative target-choice task. We used randomly-interleaved visual and olfactory cues to investigate choice-target representations. We found that

dynamic population code for choice targets evolved through the task. Systematic shift of the choice-target code represented task-periods and was meditated by neurons characterized by activation across the task-periods. Our results clarify the contribution of single-neuron responses to population dynamics, suggesting potential advantages of flexible but structured single-neuron responses as encoding strategy.

Results

We trained four rats to perform a two-alternative target-choice task where they chose a target port (left/right) associated with a presented cue to obtain reward (**Figure 1a–b**). The task performance was similar level regardless of the cue modality (mean correct rate in visual trials = 94.9±5.8 %; olfactory trials = 93.3±3.8 %). We recorded spiking activities from the PRC (n = 182 neurons) during the task performance.

The PRC neurons frequently encoded choice targets during the task performance. We used ROC analysis to generate a target-preference index which quantifies preferential responses of a neuron to a choice target. We focused on two task-periods where prominent target-encoding was observed (**Figure 1c–d**), the cue period (−400 to 0 ms before withdrawal) and the reward period (200 to 600 ms after choice), and summarized neural responses during these task-periods (**Figure 1e**). The target preference within each task-period was highly consistent across the cue modalities, indicating target processing beyond sensory modalities (r = 0.59, P < 0.001 for the cue period; r = 0.86, P < 0.001 for the reward period in **Figure 1e**). Similar amount of neurons activated in either or both of these task-periods (**Figure 1f**). Interestingly, we found that the majority of the neurons activated across both task-periods (64%; 42 of 66 neurons) dynamically changed their target-preference, while a smaller fraction (36%; 24 of 66 neurons) sustained target preference across the task periods (**Figure1 f**).

To investigate temporal dynamics of the target code, we employed a time-resolved pattern analysis (**Stokes et al., 2013**). Using this method, we decoded choice targets from the population response in a modality-independent manner (n = 182 neurons). The population code evolved through the task with two time-stable states (**Figure 2a**). Target code

was sustained during the presentation of the cue and was followed by transient response during movement toward a target port. Soon after the rats chose a target port, the target code settled again into a time-stable state (**Figure 2a**). We computed mean performance of the classifier during the cue and reward periods and compared them with the baseline (−400 to 0 ms before cue onset). As shown in **Figure 2b**, we successfully decoded choice targets in both task-periods ($P < 0.01$), indicating that the PRC tracks target information across task-periods. Furthermore, in **Figure 2c**, we found decreased target-code when we decoded choice targets using correct visual trials but erroneous olfactory trials ($n = 89$ neurons). To quantify this effect, we computed the mean classification performance in correct and erroneous trials. As shown in **Figure 2d**, the mean performance in both task-periods decreased to chance level in erroneous trials despite the fact that animals chose the same target-port as correct trials (cue period: $P \approx 0.10$; reward period: $P \approx 0.24$). These results indicate that the target code was relevant to successful task performance.

Importantly, population patterns during these two task-periods were substantially reversed (white arrows in **Figure 2a**), suggesting that the PRC distinguished different task-periods by systematic shift of the target code. We computed mean classification performance across the two task-periods and found significant shift of the target code ($P < 0.01$; **Figure 2e**). To clarify whether the shift depends on single-neuron responses or population-level structure, we shuffled the correspondence between the cue-period and reward-period responses among the neurons. This procedure resulted in collapsed shift patterns (**Figure 2e**), indicating that changes at each single-neuron level were necessary for the shift. Additionally, the shift decreased to chance level when the 20 most contributed neurons were eliminated from the population (**Figure 2f**). On the contrary, if the population was pruned randomly, the shift was preserved even after the majority of neurons were removed (**Figure 2f**). Overall, our data indicated that the PRC dynamically modified target code between task-periods and that it depended on the flexible but structured single-neuron responses.

The shift of target code is possibly signature of the encoding strategy which allows the PRC to integrate the different information, choice targets and task periods. If it is the essential nature of the PRC rather than noise, we should be able to decode richer information from neurons contributing to

the shift than the others. We therefore repeated the pattern analysis for each of the following types (classified in **Figure 1f**): neurons with shifting response, sustained response, and specific response (for either task-period). As expected, the neurons with shifting response showed clear target-code in both task-periods, as well as a dramatic change of it between the task periods (**Figure 3a**). In **Figure 3b**, we computed mean classification performance for each type and found that only neurons with shifting response showed significant performance in both task-periods ($P < 0.01$). The other types showed significant performances in the reward period ($P < 0.01$) but not in the cue period (sustained response: $P \approx 0.21$; specific response $P \approx 0.44$). Only neurons with shifting response showed significant discrimination of the task periods ($P < 0.01$; **Figure 3c**). These results underscore capacity of the PRC to integrate information across task-periods, by temporally flexible neural responses.

Discussion

In this study, we showed that the PRC dynamically encoded choice targets during task performance. We demonstrated that the target code was highly consistent across cue modality and reduced in erroneous trials. These results suggest that neural responses during the cue period might reflect retrieved target as shown by electrophysiological studies, with visual tasks, both in rodents (**Ahn and Lee, 2017**) and non-human primates (**Naya et al., 2001; Naya et al., 1996**). Our results thus provide substantial evidence for integration across sensory modalities which might support object memory.

We also found that the PRC reversed its target code between cue and reward periods. This allowed us to decode task periods as well as choice targets from the neural population. The decodability was achieved by flexible but structured single-neuron responses. Recent studies highlighted neurons with non-linear mixed selectivity which integrate different task-parameters at a given time (**Pagan et al., 2013; Raposo et al., 2014**) or across similar task-periods (e.g., Cue1 and Cue2) (**Rigotti et al., 2013**), suggesting that such complex selectivity supports functional flexibility of a brain region. Unexpectedly, our results indicate simply structured single-neuron responses across task-events and underscore their potential advantage as an

encoding strategy which reconciles different demands, keeping target information and differentiating task-events. This suggests that functional flexibility could be achieved by explicitly structured single-neuron responses. Moreover, this structured code has additional benefits. First, it can be easily read-out by downstream neurons in a consistent manner, enabling stable recognition. Second, it would support both generalization and discrimination, conflicting computations (**Barak et al., 2013**). Third, it is suitable for linking relevant information together through different time-points (**Eradath et al., 2015**), an essential computation for associative learning.

Materials and Methods

Subjects

Four male Long-Evans rats weighting 315–360 g at the beginning of training were individually housed and maintained on a laboratory light/dark cycle (lights on 8:00 A.M. to 9:00 P.M.). Rats were placed on water restriction with ad libitum access to food. The animals were maintained at 80% of their baseline weight throughout the experiments. All experiments were implemented in accordance with the guidelines for the care and use of laboratory animals provided by the Animal Research Committee of the Doshisha University.

Behavioral apparatus

The behavioral apparatus (**Figure 1a**) has been previously described (**Hirokawa et al., 2017; Osako et al., 2018**). Briefly, an operant chamber (O'Hara, Tokyo, Japan) which had three ports in the front wall for nose-poke response was enclosed in a soundproof box (Brain Science Idea, Osaka, Japan). Each port was equipped with an infrared sensor to detect animals' response. Visual cues were presented using white LEDs (4000 mcd; RS components, Yokohama, Japan) placed on the left and right walls of the operant chamber. Odors were presented via the central port through a stainless tube. Odors were mixed with pure air to produce 1:10 dilution at a flow rate of 600 ml/min using a custom-build olfactometer (AALBORG, Orangeburg, NY). Water rewards were delivered from gravity-fed reservoirs regulated by solenoid valves (The Lee Company, Westbrook, CT) through

stainless tubes placed inside of the left and right target-ports. We controlled stimulus and reward deliveries and measured behavioral responses using Bpod and Pulsepal (Sanworks LLC, Stony Brook, NY; **Sanders and Kepecs, 2014**).

Two-alternative target-choice task

Each trial started when the rats poked their snout into the central port (**Figure 1b**). After a variable delay (200–600ms), a cue pseudo-randomly selected from four stimuli (left/right LED for visual modality, S(+)/R(−)-2-octanol for olfactory modality) was presented for 1 s. If the rats successfully maintained their nose in the central port, go sound was delivered, and animals were allowed to withdraw from the central port and to choose either the left or right target-port based on the task rule (**Figure 1a**).When the rats left the center port without waiting for the go sound, the trial was canceled and followed by a 5 s punish intertrial-interval. Only correct choices were immediately rewarded by a drop of water (0.013 ml), from the target port. Rats performed typically 1018±34 trials in a daily recording session.

Training

We trained the rats step-by-step to perform the task described above. The training period typically lasted 4 to 7 weeks. First, rats were trained to poke into the central port and then collect the water reward (0.02 ml) from the left or right port. We gradually extended the duration of the poke by delaying the go sound up to 1 s after the poke onset. Next, the rats were trained to discriminate visual cues based on the same contingencies as recording sessions. A variable delay (200–600 ms) was inserted before the cue onset. After the rats became able to successfully discriminate visual cues (> 80%), they were also trained to discriminate odors based on the same contingencies as recording sessions (> 80%). Finally, we interleaved visual and olfactory trials within a session and trained the animals to perform the task to a training performance criterion (> 80%).

Mixture of odors

Cue odors, S(+)/R(−)-2-octanol, were mixed together in a subset of sessions in order to increase olfactory discrimination difficulty and thereby obtain a

246 sufficient number of erroneous trials. For instance we used a 60/40 ratio in a
247 given session, delivering odor mixture of 60% S(+)-2-octanol and 40%
248 R(−)-2-octanol. We kept odor discrimination accuracy constant (> 80%)
249 throughout recording sessions by adjusting the degree of odor mixing before
250 each session.
251
252 **Surgery**
253 Rats were anesthetized with 2.5% isoflurane before surgery, and it was
254 maintained throughout surgical procedures. We monitored body temperature,
255 movements and hind leg reflex and adjusted the depth of anesthesia as
256 needed. To keep the eyes moistened throughout the surgery, we used eye
257 ointment. Subcutaneous scalp injection of a lidocaine 1% solution provided
258 local anesthesia before the incision. The left temporalis muscle was retracted
259 to expose the skull during the surgery. A craniotomy was made over the
260 anterior part of the left PRC (AP −3.5 to −3.24 mm, ML 6.6 to 6.8 mm
261 relative to bregma, 3.5 to 4.0 mm below the brain surface) and a
262 custom-designed electrode was vertically implanted using a stereotactic
263 manipulator. A stainless screw was placed over the cerebellum and served as
264 ground during the recordings. We used the mean response of all electrodes as
265 reference. During a week of postsurgical recovery, we gradually lowered the
266 tetrodes to detect unit activities in the PRC. Electrode placement was
267 estimated based on depth and histologically confirmed at the end of the
268 experiments.
269
270 **Electrophysiological recordings**
271 A custom-designed electrode composed of eight tetrodes (tungsten wire, 12.5
272 μm, California Fine Wire, Grover Beach, CA) was used for extracellular
273 recordings. Tetrodes were individually covered by a polyimide tube (A-M
274 Systems, Sequim, WA), were placed with a 100 μm separation and typically
275 had an impedance of 250–600 kΩ at 1 kHz. Signals were recorded with
276 OpenEphys (Cambridge, MA) at a sampling rate of 30 kHz and
277 bandpass-filtered between 0.6 and 6 kHz. Tetrodes were lowered
278 approximately 80 μm after each recording session, and thereby independent
279 populations of neurons were recorded across sessions.
280
281 **Spike sorting and screening criteria of units**

All analyses were performed in Matlab (Mathworks, Natick, MA). To detect single-neuron responses, spikes were manually clustered with MClust (A.D. Redish) for Matlab. Only neurons met the following criteria in further analyses: (1) units with reliable refractory period (violations were less than 1% of all spikes); and (2) units with sufficient mean firing rate in the 1 s after the cue onset (> 0.5 Hz).

Selective response to choice targets

In order to evaluate selective responses to choice targets, we calculated a target-preference index (**Hirokawa et al., 2011**). We first grouped correct trials into four types based on cue modality (visual or olfactory) and target choice (left or right). For each modality, we independently calculated the target preference, using ROC analysis (**Green and Swets, 1966**). The target -preference index was obtained from the area under ROC curve (AUC) and defined as 2×(AUC−0.5) ranging from −1 to 1. In our analysis, a positive value indicated a neuron selectively fired to left target-choice, and a negative value indicated the opposite. A value of zero showed the absence of selective responses. To determine statistical significance (one-tailed, $P < 0.05$), we used bootstrapping (100 interactions).

Decoding analysis statistics

We evaluated statistical significance of decoding analysis with bootstrapping procedure (**Ojala and Garriga, 2010; Parthasarathy et al., 2017**). Two bootstrapped distributions whose 95th ranges for mean did not overlap were considered as significantly different. We estimated the P value for this bootstrapping procedure by computing the ratio $(1+X)/(N+1)$ between the number X of overlapping data points between the two distributions and the number N of interactions (**Ojala and Garriga, 2010; Parthasarathy et al., 2017**). Since we used 100 bootstraps throughout all decoding analyses, two distributions with no overlap resulted in $P < 0.01$, and two distributions with x % overlap resulted in $P \approx x/10$.

Decoding analysis

We employed cross-temporal pattern analysis (**Stokes et al., 2013; Wasmuht et al., 2018**) to investigate the temporal dynamics of the target code by neural population in the PRC. Neural responses were pooled across

recording sessions to maximize the number of neural responses included in the decoding analysis. Here we refer to the pooled pseudo-population of the PRC neurons (n = 182) as full population. The instantaneous firing rate of each neuron was estimated by spike counts in a 150 ms sliding window (10 ms increment). We converted the instantaneous firing rates for each neuron into the target-preference index independently calculated for visual and olfactory trials. In this manner, we generated two independent population vectors for the full population (cell×time vector each for the cue modalities). We obtained a pattern similarity index by calculating the Fisher-transformed Pearson correlation (r) between these two population vectors. This index provided the pattern similarity for both equivalent and different time points (e.g., **Figure 2a**). A positive correlation was interpreted as an evidence for reliable target code irrespective of the cue modality.

To estimate mean performance values for the pattern classification analysis, we pseudo-randomly resampled neurons (the same number of neurons as neural population analyzed) and computed the target preference in visual and olfactory trials. Neural responses were aligned to withdrawal onset (from the central port) and target-choice onset (left or right). This enabled us to calculate pattern similarity indices within and across the two task-periods that were main focus of our study, the cue and the reward periods. We repeated this process 100 times to obtain a distribution of 100 different measurements of the pattern classification. To investigate neural responses during the task periods, we averaged the performance within the cue period and reward period (e.g. **Figure 2b**). To obtain a baseline performance, we averaged the classification performance during the baseline period, −400 to 0 ms before the cue onset. We also quantified the temporal change of neural responses between these task-periods by averaging the following two pattern classifications: pattern classification for cue-period responses in visual trials and reward-period responses in olfactory trials, and cue-period responses in olfactory trials and reward-period responses in visual trials (e.g. **Figure 2e**). We calculated the 95th percentile range for each of distribution. If the 95th range of 100 different pattern classification measurements within a task period did not overlap with the 95th range of baseline distribution, we considered the choice targets to be decodable from the neural population response during the task event. We considered zero to be chance level instead of the baseline distribution when we checked

statistical significance of the classification across the task periods.

Decoding analysis of erroneous trials

We included 89 neurons recorded in sessions with sufficient number of erroneous choices (at least 11 trials for both choice targets) in all analyses for erroneous trials. Due to the similarity of the target preference between different cue modalities in correct trials, we calculated the pattern similarity index using correct visual trials and erroneous olfactory trials to evaluate influence of erroneous behavioral performance on target code (**Figure 2c**). We computed mean performance of the pattern classification in correct and erroneous trials (**Figure 2d**).

Contribution of single-neuron responses to population level shift

We quantified changes of the target code between the task-periods with n−1 neural population by excluding one neuron from the full population and repeating this procedure 182 times. This enabled us to directly quantify how strongly each neuron contributed to the shift and to sort the neurons in decreasing order of contribution level. We gradually eliminated neurons that highly contributed to the shift from the full population. In this manner, we computed the classification performance across the task-periods as a function of the number of neurons excluded from the neural population (**Figure 2f**). This was compared with the 95th percentile range of a control distribution obtained by randomly eliminating neurons from the population (100 repetitions).

Role of different types of neurons

We randomly selected 24 neurons each for three different types of the target code (defined by target preference in the cue period and the reward period) and performed the pattern classification analysis for each type of neuron: (ⅰ) neurons with shifting response, (ⅱ) neurons with sustained response, and (ⅲ) neurons with specific response (**Figure 3b–c**). We combined 12 neurons which showed significant target preference in the cue period and 12 neurons which showed significant target preference in the reward period into subpopulations of neurons with specific response.

Author contributions

T.O., Y.S., and J.H. designed the experiments. T.O. performed the experiments and analyzed data. Y.O. analyzed data. H.M, Y.S. and J.H. supervised the project. All authors contributed to writing the manuscript.

Conflict of Interest Statement

The authors declare no competing interests.

Acknowledgments

We would like to thank members of Laboratory of Neural Information at Doshisha University for helpful discussions, and Y. Tanisumi for help with visualization of data. This research was supported by the Research Grants KAKENHI 16H02061 and 18H0588 (to Y.S.) and 16K18380 (to J.H.).

References

Ahn JR, Lee I. 2017. Neural Correlates of Both Perception and Memory for Objects in the Rodent Perirhinal Cortex. *Cereb Cortex* **27**:3856–3868. doi:10.1093/cercor/bhx093

Ahn JR, Lee I. 2015. Neural Correlates of Object-Associated Choice Behavior in the Perirhinal Cortex of Rats. *J Neurosci* **35**:1692–1705. doi:10.1523/JNEUROSCI.3160-14.2015

Barak O, Rigotti M, Fusi S. 2013. The sparseness of mixed selectivity neurons controls the generalization-discrimination trade-off. *J Neurosci* **33**:3844–3856. doi:10.1523/JNEUROSCI.2753-12.2013

Burwell RD. 2001. Borders and cytoarchitecture of the perirhinal and postrhinal cortices in the rat. *J Comp Neurol* **437**:17–41. doi:10.1002/cne.1267

Burwell RD, Amaral DG. 1998. Perirhinal and postrhinal cortices of the rat: Interconnectivity and connections with the entorhinal cortex. *J Comp Neurol* **391**:293–321. doi:10.1002/(SICI)1096-9861(19980216)391:3<293::AID-CNE2>3.0.CO;2-X

Elsayed GF, Lara AH, Kaufman MT, Churchland MM, Cunningham JP. 2016. Reorganization between preparatory and movement population responses in motor cortex. *Nat Commun* **7**:13239. doi:10.1038/ncomms13239

Eradath MK, Mogami T, Wang G, Tanaka K, Eradath XMK, Mogami T, Wang G, Tanaka K. 2015. Time context of cue-outcome associations represented by neurons in perirhinal

cortex. *J Neurosci* **35**:4350–4365. doi:10.1523/jneurosci.4730-14.2015

Furtak SC, Wei S-M, Agster KL, Burwell RD. 2007. Functional Neuroanatomy of the Parahippocampal Region in the Rat: The Perirhinal and Postrhinal Cortices. *Hippocampus* **17**:709–722. doi:10.1002/hipo

Furuyashiki T, Holland PC, Gallagher M. 2008. Rat orbitofrontal cortex separately encodes response and outcome information during performance of goal-directed behavior. *J Neurosci* **28**:5127–5138. doi:10.1523/JNEUROSCI.0319-08.2008

Gardner MPH, Fontanini A. 2014. Encoding and Tracking of Outcome-Specific Expectancy in the Gustatory Cortex of Alert Rats. *J Neurosci* **34**:13000–13017. doi:10.1523/JNEUROSCI.1820-14.2014

Green DM, Swets JA. 1966. Signal Detection Theory and Psychophysics. Wiley, New York.

Guo Z V., Inagaki HK, Daie K, Druckmann S, Gerfen CR, Svoboda K. 2017. Maintenance of persistent activity in a frontal thalamocortical loop. *Nature* **545**:181–186. doi:10.1038/nature22324

Hirokawa J, Sadakane O, Sakata S, Bosch M, Sakurai Y, Yamamori T. 2011. Multisensory information facilitates reaction speed by enlarging activity difference between superior colliculus hemispheres in rats. *PLoS One* **6**. doi:10.1371/journal.pone.0025283

Hirokawa J, Vaughan A, Kepecs A. 2017. Categorical representations of decision-variables in orbitofrontal cortex. *bioRxiv*. doi:10.1101/135707

Hosokawa T, Kato K, Inoue M, Mikami A. 2005. Correspondence of cue activity to reward activity in the macaque orbitofrontal cortex. *Neurosci Lett* **389**:146–151. doi:10.1016/j.neulet.2005.07.055

Kennerley SW, Wallis JD. 2009. Evaluating choices by single neurons in the frontal lobe: Outcome value encoded across multiple decision variables. *Eur J Neurosci* **29**:2061–2073. doi:10.1111/j.1460-9568.2009.06743.x

Kepecs A, Uchida N, Zariwala HA, Mainen ZF. 2008. Neural correlates, computation and behavioural impact of decision confidence. *Nature* **455**:227–231. doi:10.1038/nature07200

Lara AH, Cunningham JP, Churchland MM. 2018. Different population dynamics in the supplementary motor area and motor cortex during reaching. *Nat Commun* **9**. doi:10.1038/s41467-018-05146-z

Mante V, Sussillo D, Shenoy K V, Newsome WT. 2013. Context-dependent computation by recurrent dynamics in prefrontal cortex. *Nature* **503**:78–84. doi:10.1038/nature12742

Naya Y, Chen H, Yang C, Suzuki WA. 2017. Contributions of primate prefrontal cortex and medial temporal lobe to temporal-order memory. *Proc Natl Acad Sci U S A* **114**:13555–13560. doi:10.1073/pnas.1712711114

Naya Y, Sakai K, Miyashita Y. 1996. Activity of primate inferotemporal neurons related to a sought target in pair-association task. *Proc Natl Acad Sci U S A* **93**:2664–2669. doi:10.1073/pnas.93.7.2664

Naya Y, Suzuki WA. 2011. Integrating what and when across the primate medial temporal lobe. *Science* **333**:773–776. doi:10.1126/science.1206773

Naya Y, Yoshida M, Miyashita Y. 2003a. Forward processing of long-term associative memory in monkey inferotemporal cortex. *J Neurosci* **23**:2861–2871. doi:10.1523/JNEUROSCI.23-07-02861.2003

Naya Y, Yoshida M, Miyashita Y. 2001. Backward spreading of memory-retrieval signal in the primate temporal cortex. *Science* **291**:661–664. doi:10.1126/science.291.5504.661

Naya Y, Yoshida M, Takeda M, Fujimichi R, Miyashita Y. 2003b. Delay-period activities in two subdivisions of monkey inferotemporal cortex during pair association memory task. *Eur J Neurosci* **18**:2915–2918. doi:10.1046/j.1460-9568.2003.03020.x

Ohyama K, Sugase-Miyamoto Y, Matsumoto N, Shidara M, Sato C. 2012. Stimulus-related activity during conditional associations in monkey perirhinal cortex neurons depends on upcoming reward outcome. *J Neurosci* **32**:17407–17419. doi:10.1523/JNEUROSCI.2878-12.2012

Ojala M, Garriga GC. 2010. Permutation Tests for Studying Classi er Performance. *J ofMachine Learn Res* **11**:1833–1863. doi:10.1109/ICDM.2009.108

Osako Y, Sakurai Y, Hirokawa J. 2018. Subjective decision threshold for accurate visual detection performance in rats. *Sci Rep* **8**:1–10. doi:10.1038/s41598-018-27696-4

Pagan M, Urban LS, Wohl MP, Rust NC. 2013. Signals in inferotemporal and perirhinal cortex suggest an untangling of visual target information. *Nat Neurosci* **16**:1132–1139. doi:10.1038/nn.3433

Parthasarathy A, Herikstad R, Bong JH, Medina FS, Libedinsky C, Yen S. 2017. Mixed selectivity morphs population codes in prefrontal cortex **20**. doi:10.1038/s41593-017-0003-2

Qu LP, Kahnt T, Cole SM, Gottfried JA. 2016. De Novo Emergence of Odor Category Representations in the Human Brain. *J Neurosci* **36**:468–478. doi:10.1523/JNEUROSCI.3248-15.2016

Raposo D, Kaufman MT, Churchland AK. 2014. A category-free neural population supports evolving demands during decision-making. *Nature***17**:1784–1792. doi:10.1038/nn.3865

Rigotti M, Barak O, Warden MR, Wang X-J, Daw ND, Miller EK, Fusi S. 2013. The importance of mixed selectivity in complex cognitive tasks. *Nature* **497**:585–590. doi:10.1038/nature12160

Sakai K, Miyashita Y. 1991. Neural organization for the long-term memory of paired

associates. *Nature* **354**:152–155. doi:10.1038/354152a0

Sakurai Y. 1990a. Hippocampal cells have behavioral correlates during the performance of an auditory working memory task in the rat. *Behav Neurosci* **104**:253–263. doi:10.1037/0735-7044.104.2.253

Sakurai Y. 1990b. Cells in the rat auditory system have sensory-delay correlates during the performance of an auditory working memory task. *Behav Neurosci* **104**:856–868. doi:10.1037/0735-7044.104.6.856

Sakurai Y., Ohnuki T, Shiroshita R., Sakaguchi Y., Shiotani K, Lee CJ. 2017. Multipotentiality of the brain to be revisited repeatedly. Eds. Opris I, Casanova MF. The physics of the mind and brain disorders: 513-525. Springer series in cognitive and neural systems, **11**. Springer, Cham. doi: 10.1007/978-3-319-29674-6_23

Sanders JI, Kepecs A. 2014. A low-cost programmable pulse generator for physiology and behavior. *Front Neuroeng* **7**:1–8. doi:10.3389/fneng.2014.00043

Stokes MG, Kusunoki M, Sigala N, Nili H, Gaffan D, Duncan J. 2013. Dynamic coding for cognitive control in prefrontal cortex. *Neuron* **78**:364–375. doi:10.1016/j.neuron.2013.01.039

Taylor KI, Moss HE, Stamatakis EA, Tyler LK. 2006. Binding crossmodal object features in perirhinal cortex. *Proc Natl Acad Sci U S A* **103**:8239–8244. doi:10.1073/pnas.0509704103

Tomás Pereira I, Agster KL, Burwell RD. 2016. Subcortical connections of the perirhinal, postrhinal, and entorhinal cortices of the rat. I. afferents. *Hippocampus* **26**:1189–1212. doi:10.1002/hipo.22603

Wasmuht DF, Spaak E, Buschman TJ, Miller EK, Stokes MG. 2018. Intrinsic neuronal dynamics predict distinct functional roles during working memory. *Nat Commun* **9**. doi:10.1038/s41467-018-05961-4

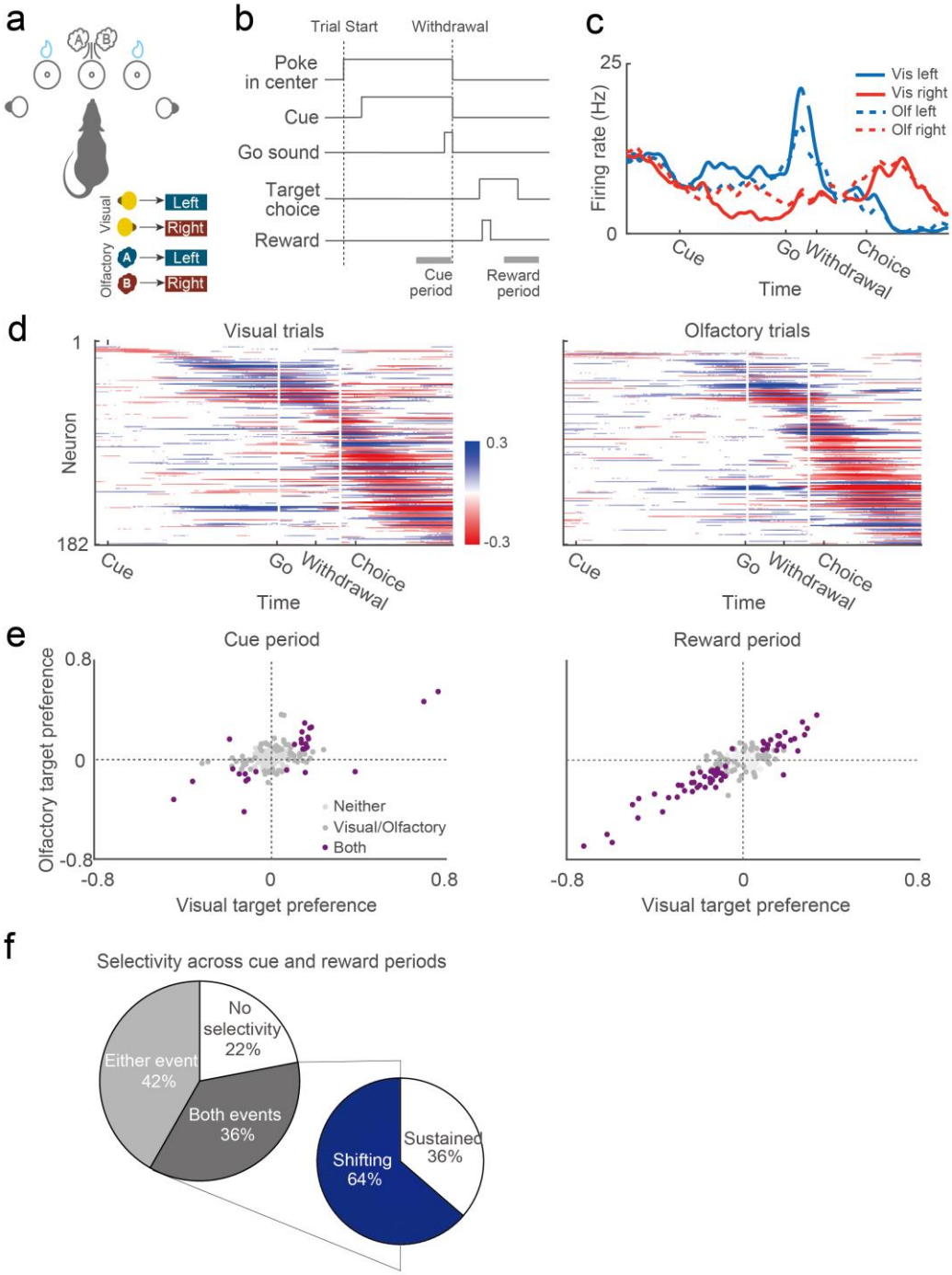

Figure 1. The PRC neurons encoded choice targets. (**a**) Schematic drawing of behavioral apparatus and cue-target associative relationships. (**b**) Schematic of the task timeline. Bars represent two 400 ms task-periods. (**c**) Peri-stimulus time histograms showing the activity of a representative neuron throughout the task. Trial types are classified according to cue

529 modality and target choice as follows: blue, left target-choice; red, right
530 target-choice; solid line, visual trials; dashed line; olfactory trials. Mean
531 firing rates for each of the four trial types were computed in 10 ms time
532 windows (smoothed with a Gaussian, σ = 30 ms). Neural responses were
533 independently aligned to cue, withdrawal and target-choice onset and then
534 reconstructed because of variable time between them. Only correct trials
535 were included. (**d**) Temporal patterns of choice-target selective responses of
536 the PRC neurons (n = 182) in visual (left) and olfactory trials (right). Mean
537 firing rates were smoothed with a Gaussian (σ = 150 ms) and then converted
538 into a target-preference index. Positive values (blue) indicate selective
539 firings to leftward choices, and negative values (red) indicate selective firings
540 to rightward choices. For each modality, neurons were independently sorted
541 according to the time of their peak response. Only segments with significant
542 target preference were shown ($P < 0.05$; 1,000 bootstraps). (**e**) Scatter plots
543 showing target preference of the neural population in the cue (left) and
544 reward (right) periods. Each point corresponds to values of a single neuron.
545 Colors indicate significance: light gray, no selectivity; deep gray, significant
546 in either cue modality; purple significant in both cue-modalities. (**f**)
547 Distribution of neurons with different types of choice-target selective
548 response across the cue and reward periods.

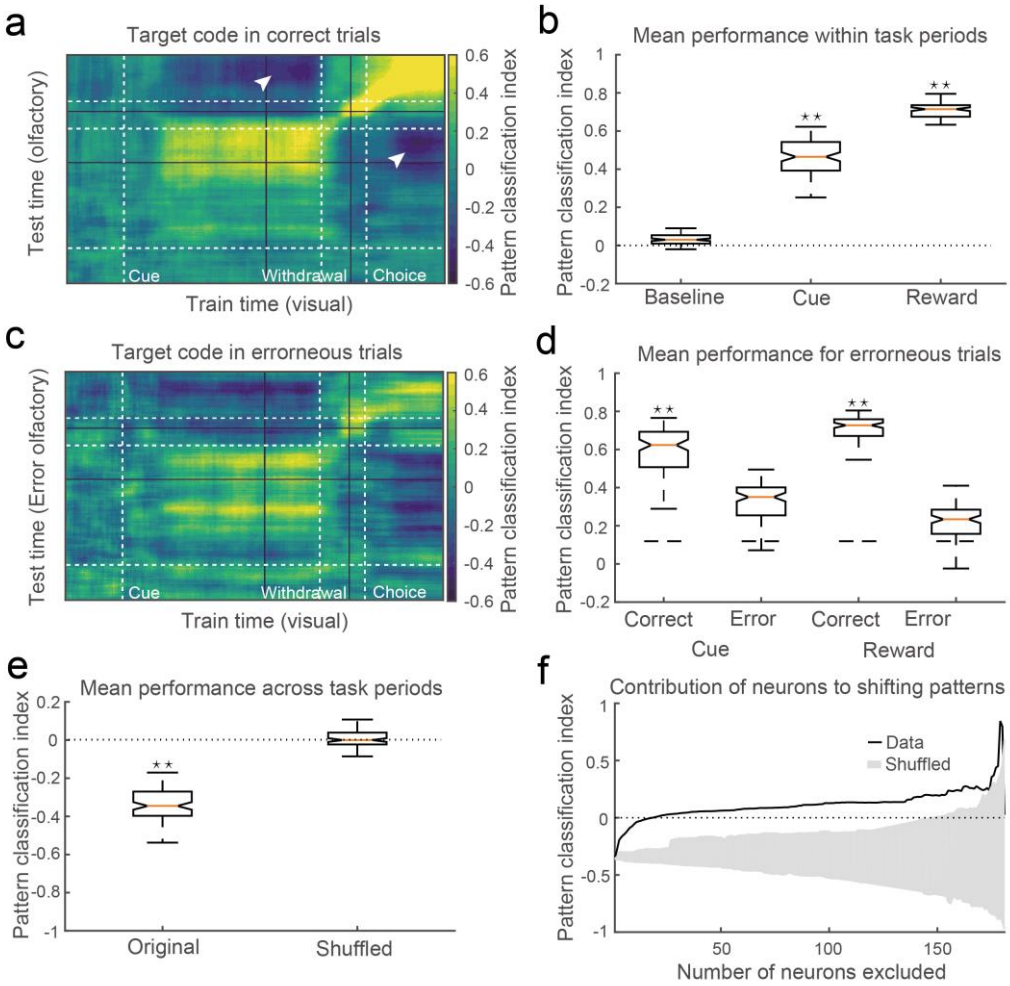

Figure 2. Time-resolved pattern analysis for choice-target code. (**a**) Heat map showing performance of the pattern classification analysis. White lines correspond to the onset time of cue, withdrawal, and target choice. We trained classifiers using neural responses in correct visual trials to discriminate choice targets and tested them with neural responses in correct olfactory trials (n = 182 neurons). (**b**) Mean classification performance during the baseline, cue and reward periods. (**c**) A classifier tested with erroneous olfactory trials (n = 89 neurons). (**d**) Mean classification performance for erroneous trials. Dashed lines indicate the 97.5th percentile value of a baseline distribution. (**e**) Mean classification performance across the cue and reward periods for original data and data with shuffled correspondence of those periods (n = 182 neurons). (**f**) Classification performances with decreasing number of neurons, removed from most to least contributed to the shift of target code. Original data is indicated as a black line. Gray shaded

area indicates 95th percentile range of data with shuffled order of neurons (100 shuffles). In box plots: center orange line, median; box limits, 25th and 75th quartiles; notch limits, (1.57×interquartile range)/√n; whiskers, 95th percentile range (two-sided) of the distribution. Asterisks indicate statistical significance (P < 0.01): the 95th percentile range of the performance distribution did not overlap with the 95th percentile range of a baseline distribution (for classification performances within a task period) or zero (for classification performances across two task-periods).

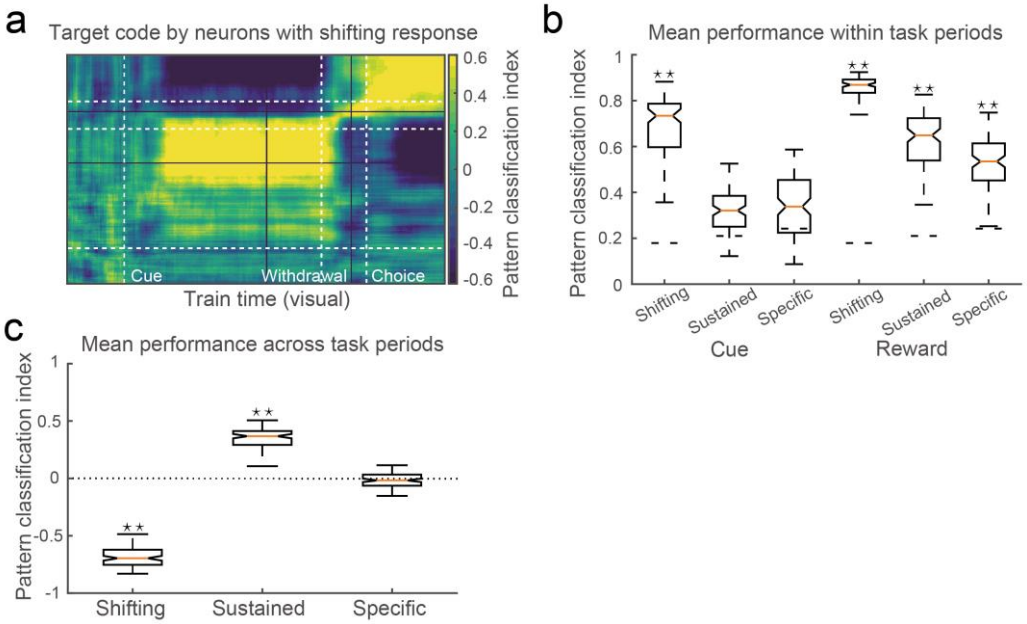

Figure 3. Roles of different types of neurons in target code. (**a**) Heat map showing performance of a classifier trained and tested using neural responses with shifting target preference between the cue- and reward period (n = 42 neurons). (**b**) Mean classification performance with three different types of neurons. 24 neurons were included in each different type. Dashed lines indicate the 97.5th percentile value of the baseline distribution. (**c**) Mean classification performances across the two task-periods. In box plots: center orange line, median; box limits, 25th and 75th quartiles; notch limits, (1.57×interquartile range)/√n; whiskers, 95th percentile range (two-sided) of the distribution. Asterisks indicate statistical significance (P< 0.01): the 95th percentile range of a performance distribution did not overlap with the 95th percentile range of a baseline distribution (for classification performances within a task period) or zero (for classification performances across two task- periods).